Supplementary Information for

In operando, photovoltaic, microscopic evaluation of recombination centers in halide perovskite-based solar cells

Arava Zohar[*], Michael Kulbak[*], Silver H. Turren-Cruz[§¥], Pabitra K. Nayak[†+], Adi Kama[‡], Anders Hagfeldt[§], Henry J Snaith[†], Gary Hodes[*], David Cahen[*‡]

[*]Dept. of Materials and Interfaces, Weizmann Inst. of Science, Rehovot 76100, Israel
[‡]Chem. Dept. and Inst. for Nanotechn. & Adv. Mater., Bar-Ilan Univ., Ramat Gan 52900, Israel

[§]École Polytechnique Fédérale de Lausanne, CH-1015-Lausanne, Switzerland.

[¥]Inst. of Advanced Materials (INAM), Jaume I University, Castelló de la Plana 12071, Spain

[†]Dept. of Physics, Clarendon Lab., Univ. of Oxford, Oxford, OX1 3PU, UK

[+]Tata Institute of Fundamental Research 36/P, Gopanpally Village, Serilingampally Mandal, Ranga Reddy District, Hyderabad 500046, India

Part A – EBIC method setup

The EBIC method is based on the current of electrons excited by an electron beam, similar to the photovoltaic effect. One of the main features of this method is the ability to visualize the electric field in a working solar cell. A photovoltaic cell efficiency will depend on the electric field (profile and intensity) and electronic transport properties for a given semiconductor. The former stems from the densities and the nature (p or n) of the dopants (intrinsic or extrinsic electrically active defects), and the latter reflects the mobility–lifetime product. The EBIC signal is the collected current at the electrodes from the sample, which can be a full solar cell, as in our case here. This current will be highest from volumes within which electron-hole pairs are generated by the electron beam, from where charge separation and charge collection are most efficient. In most cases, these volumes will be within the space charge region (SCR) as the electric field in that region removes charges rapidly, leading to charge depletion and hence, lower recombination. The electric field profile extracted from the EBIC signal can provide information on the nature of the doping and, by using a suitable model, we can estimate the doping density. From the decay of the EBIC signal the minority carrier diffusion length can be estimated, as we did for halide perovskites in earlier work. In a further use of EBIC in the study of halide perovskites the role of grain boundaries in carrier recombination was

studied[1,2] and effects of alkali cations in/on halide perovskites were deduced[3]. A schematic of our set-up is given in Figure S1.

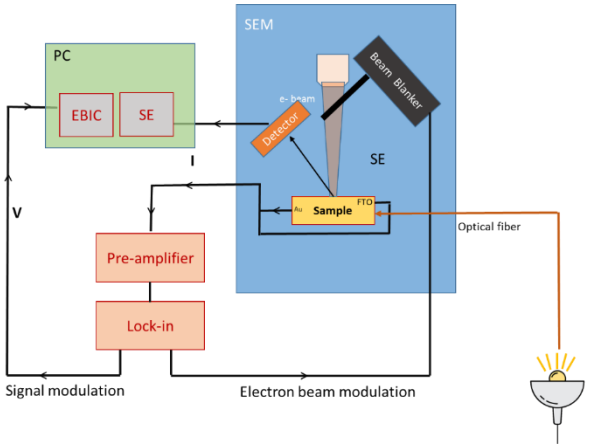

Fig. S1 *– Scheme of the EBIC setup with background illumination. The blue panel represents the electron microscopy chamber. The external light source was coupled to a 600 μm diameter optical fiber via dedicated vacuum connectors. The end-point of the optical fiber is fixed to the optically transparent side of the solar device. The generation rates, G, were calculated based on HaP thickness and the light intensity at the end of the fiber, which was measured with a silicon photodiode.*

Samples are cleaved in an inert atmosphere and measured right away, with minimal exposure of the exposed cell cross-section to the atmosphere until the sample is in the high vacuum of the SEM chamber.

The collected EBIC was between 20-50 nA in the dark. The EBIC signal with background illumination was measured using a beam blanker (BB) with a frequency of 60kHz and a lock-in amplifier to improve the signal-to-noise ratio. As an outcome, the collected current was lower; 1-5 nA under illumination. We used the BB only for the illuminated samples since the quality of the SE image with the BB is poor compared to that without BB.

We can evaluate E in the cell's cross-section by the built-in potential: the regularly measured voltage for a cross-section sample is 1 V for MAPI and 500 mV for Br-based perovskite cells. Therefore, the E should be in the range of 2-3x10^4 V/cm.

The generation rate, G, represents the e-h carrier generation rate, in units of [photons/ (cm^3 sec)]. G was calculated by applying the light source intensity (P) in W/cm^2 equation 1.

$$G = \frac{P}{h\nu * l} = \frac{0.010\left[\frac{W}{cm^2}\right]}{3.14 \times 10^{-19}\left[\frac{J}{photon}\right] 3 \times 10^{-5}[cm]} \times 0.8 = 8.5 \times 10^{20}\left[\frac{1}{cm^3 s}\right] \quad \text{(S1)}$$

Where l is the thickness of the films, hν is the photon energy in Joule/photon, and P is the measured light score power in mW/cm^2. The HaP thickness was measured for each cross-section by SE imaging (~300 nm). The net absorbed light was multiplied by a factor of ~0.8 to account for reflection losses and the limitation of the quantum efficiency.

Part B- EBIC analysis

The formula for fitting the EBIC data to extract L_d is the following:

$$y = y_0 + Ae^{\left(\frac{x_0 - x}{L_n}\right)} \quad \text{(S2)}$$

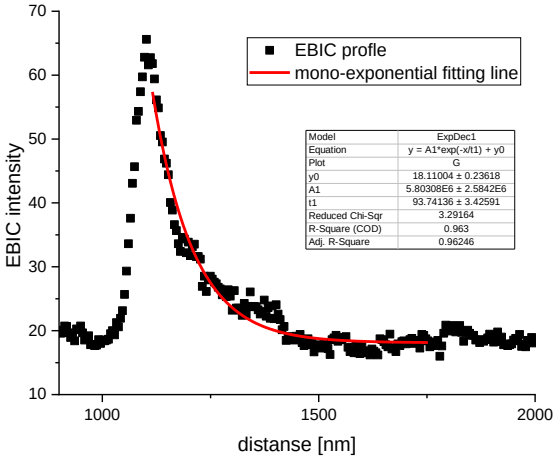

Fig. S2 *– An example of the fit the above relation (red curve) to the EBIC signal to get L_d. The black dots are the EBIC profile line as a function of spatial coordinate. The red line is the fit to a monoexponential decay. The "y" in the formula represents the EBIC intensity as a function of spatial coordinate (x_o-x) in the formula.*

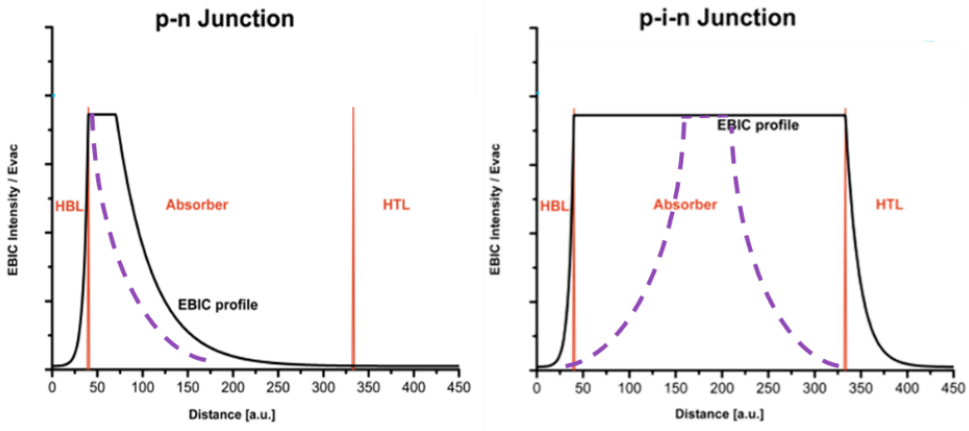

Fig S3 –Schematic of the EBIC signals for a p-n (p-doped HaP) or p-i-n (intrinsic HaP) junction cases, with long (black solid line) or short (dashed purple line) L_d. This drawing was taken from Kedem et al.[4]

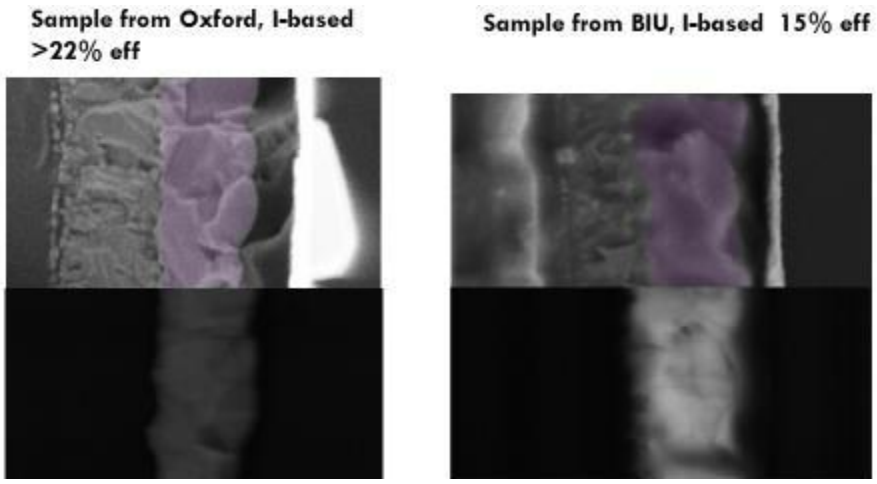

$Cs_{0.17}FA_{0.83}Pb(I_{0.6}Br_{0.4})_3$ **$Cs_{0.05}MA_{0.16}FA_{0.79}Pb(I_{0.84}Br_{0.16})_3$**

Fig. S4 *- SE image, (top) and corresponding EBIC image (bottom) of cross-sections of PV devices made with iodide-based perovskites made at (a) Oxford (b) Bar-Ilan University. The selective contacts are FTO/d-TiO_2 and mp-TiO_2/HaP (written on the bottom of the EBIC Image) /hole transport layer/Au. The halide perovskite is colored purple in the SE images.*

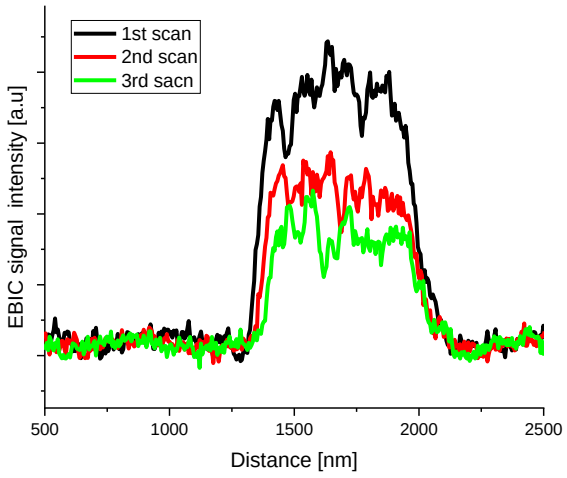

Fig. S5 *- EBIC line scans of the cross section of FTO/d-TiO_2 / mp-TiO_2/MAFAPbI_3 /hole transport layer/Au made at Bar-Ilan Univ. The EBIC signal of the same region decreased by a factor of two for an electron-beam voltage of 2 kV due to beam damage. Still, the position of the EBIC signal did not change from scan to scan, i.e., the HaP shows a uniform field regardless of the beam damage.*

Part C - Sample preparation - BIU (WIS, EPFL, and Oxford procedure can be found in ref [5–7])

The TiO_2 Layer: Fluorine doped tin oxide (FTO, KINTEC Company) coated glass substrates (TEC 15, 72 mm × 72 mm) were cleaned in a sonication bath with soap (Decon 90), deionized water, rinsed in dry ethanol, and washed again with deionized water. The substrate was then treated with an Ar plasma for 4 min. The TiO_2 blocking layer was deposited by spray pyrolysis (custom-made).[8] The substrate was placed on a hotplate heated to 450 °C. The TiO_2 precursor solution was prepared by mixing 7.5 mL of titanium-tetra-isopropoxide (TTiP, Sigma-Aldrich) and 5 mL of acetylacetone (Sigma-Aldrich) in 240 mL of ethanol (Carlo Erba Reagents), and its pH was 6.8. The precursor solution was sprayed at a rate of 0.4 ml/sec to thickness of 30 nm. The 100-150 nm thick mesoporous TiO_2 scaffold was spin-coated on the TiO_2 blocking layer from diluted nanoparticle paste (18NR-T Dyesol) diluted with absolute ethanol at a weight ratio of 1:10 and sintered at 550 °C for 1.5 h.

The Absorber layer, $Cs_{0.05}MA_{0.16}FA_{0.79}Pb(I_{0.84}Br_{0.16})_3$: This was prepared using CsI 99.9% and PbI_2 99% (Sigma Aldrich), MABr, and FAI (Greatcell Solar) and $PbBr_2$ (TCI). 1.5 M of CsI was

dissolved in DMSO (N,N-dimethylformamide, dimethyl sulfoxide), 1.5 M solution of $PbBr_2$, and PbI_2, was dissolved using 4:1 ratio of DMF : DMSO at 180º C for 15 min. Equimolar powders of MABr and FAI were dissolved in $PbBr_2$ and PbI_2 solutions, respectively, to form 1.5 M of $MAPbBr_3$ and $FAPbI_3$. The final solution was prepared using 79% of $FAPbI_3$, 16% $MAPbBr_3$, and 5% CsI. 200µL of the final solution $Cs_{0.05}MA_{0.16}FA_{0.79}Pb(I_{0.84}Br_{0.16})_3$ was spin-coated at 5000 RPM for 30 seconds with 300µL chlorobenzene anti-solvent drip after 20 sec. The resulting films were annealed at 100 °C for 1 hour.

A 36 mM solution of spiro-OMeTAD (1-Material Inc.) was dissolved in chlorobenzene with additives, tris(2- (1Hpyrazol-1-yl) -4-tert-butylpyridine) cobalt (III), tri [bis (trifluoromethane) sulfonimide] (FK209, Sigma Aldrich), bis (trifluoromethane)sulfonimide lithium salt (LiTFSI) that were dissolved in acetonitrile, and 1% of 4-tertbutylpyridine (tBP). 150µL of spiro solution was spin-coated on the perovskite film. 80 nm thick gold contacts were deposited by thermal evaporation at a rate of 0.05 nm/sec.

Part D- Rose model (cf. refs. 9, 10)

The numerical solution for the set of equations (Rose model) describes a slightly p-type semiconductor and a steady-state illumination, and a known rate of generation and capture (or recombination) was found by a Matlab code attached below

```
function OUT = Ge_rate_01(Gpass, NrVar)
    syms x y z;

%%%%%%%%%%%%%%%%%%%%%%%%%%%%%%%%%%%%%%%%%%%%%%%%%%%%%%%%%%%%%%%%
%%%%%%%%%%
    A   = NrVar; %1*10^(11);   % N_r
    B   = 10^(-8);   % C_e
    C   = 10^(-6);   % C_h
    D   = 5*10^(-10);   %C_bi
    G   = Gpass;
    P10 = 10^(11); % initially trapped minority carrier
concentration
```

```
%%%%%%%%%%%%%%%%%%%%%%%%%%%%%%%%%%%%%%%%%%%%%%%%%%%%%%%%%%%%%%%%%%%%%%%%%%%%%%%%%%%
    eq1  =  x-y+z+P10;  %x=n; y=p; z=n_r
    eq2a = (A*B*x);
    eq2b = (B*x)+(C*y);
    eq2  =  eq2a/eq2b;
    eq3  = (C*y*z)+(D*x*y);
    EqNs = [eq1==A, eq2==z, eq3==G] ;
```

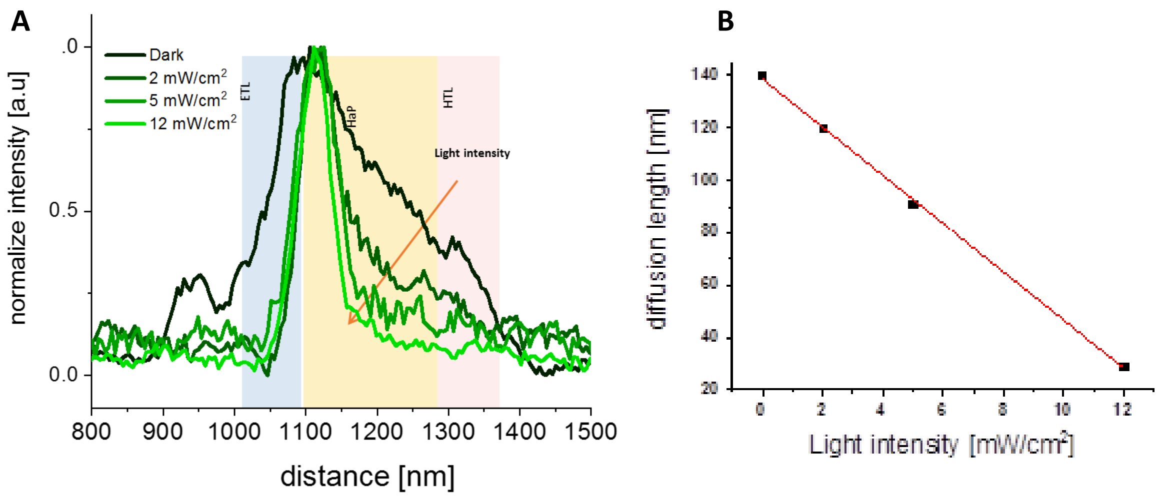

Fig. S6 *– A) EBIC line scans of the cross-section and B) the extracted diffusion length of FTO/ d-*TiO_2 *and mp-*TiO_2*/MAFACsPbBr*$_3$ */PTAA/Au, made by the WIS group, under various background illumination intensities. The signal intensities were normalized because the signal amplification was changed between scans. The position of the maximum EBIC signal intensity was at the* TiO_2*/HaP interface. The EBIC signal decays faster as background illumination intensity increases.*

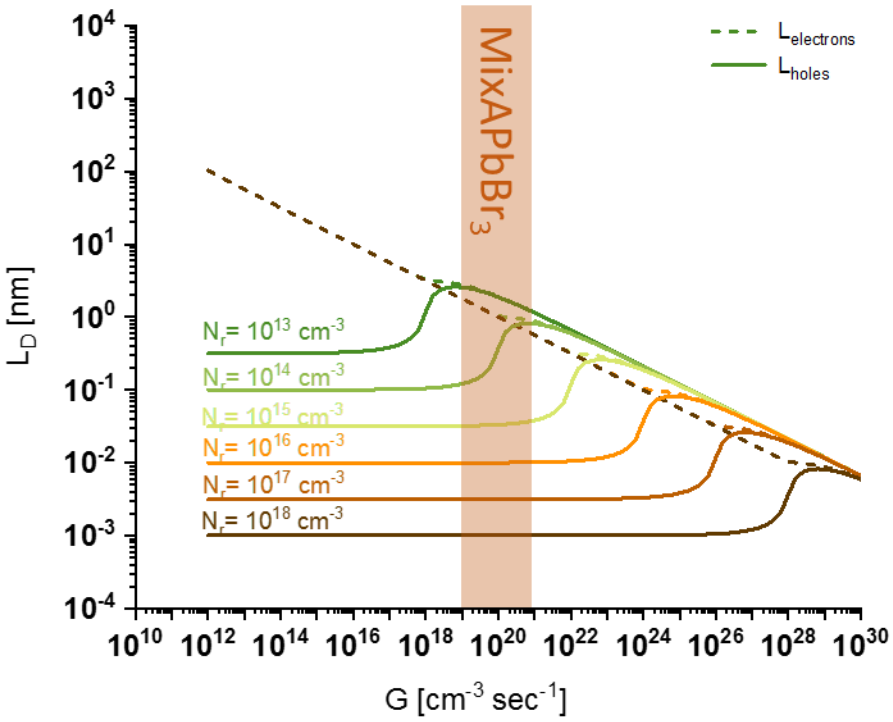

Fig. S7 *- Diffusion lengths, L_D, of both charge carrier types, as a function of the photogeneration rate, G, as derived numerically, using the single effective trap state, Rose model*[9,10] *for MAPbBr$_3$(Cl) films.*

References

(1) Seo, G.; Lee, D.; Heo, S.; Seol, M.; Lee, Y.; Kim, K.; Kim, S. H.; Lee, J.; Lee, D.; Lee, J.; Kwak, D. W.; Lee, D.; Cho, H. Y.; Park, J.; Ahn, T. K.; Nazeeruddin, M. K. Microscopic Analysis of Inherent Void Passivation in Perovskite Solar Cells. *ACS Energy Lett.* **2017**, *2* (7), 1705–1710. https://doi.org/10.1021/acsenergylett.7b00484.

(2) Yang, B.; Dyck, O.; Poplawsky, J.; Keum, J.; Puretzky, A.; Das, S.; Ivanov, I.; Rouleau, C.; Duscher, G.; Geohegan, D.; Xiao, K. Perovskite Solar Cells with Near 100% Internal Quantum Efficiency Based on Large Single Crystalline Grains and Vertical Bulk Heterojunctions. *J. Am. Chem. Soc.* **2015**, *137* (29), 9210–9213. https://doi.org/10.1021/jacs.5b03144.

(3) Correa-Baena, J.-P.; Luo, Y.; Brenner, T. M.; Snaider, J.; Sun, S.; Li, X.; Jensen, M. A.; Hartono, N. T. P.; Nienhaus, L.; Wieghold, S.; Poindexter, J. R.; Wang, S.; Meng, Y. S.; Wang, T.; Lai, B.; Holt, M. V.; Cai, Z.; Bawendi, M. G.; Huang, L.; Buonassisi, T.;

Fenning, D. P. Homogenized Halides and Alkali Cation Segregation in Alloyed Organic-Inorganic Perovskites. *Science* **2019**, *363* (6427), 627–631. https://doi.org/10.1126/science.aah5065.

(4) Kedem, N.; Brenner, T. M.; Kulbak, M.; Schaefer, N.; Levcenko, S.; Levine, I.; Abou-Ras, D.; Hodes, G.; Cahen, D. Light-Induced Increase of Electron Diffusion Length in a p–n Junction Type $CH_3NH_3PbBr_3$ Perovskite Solar Cell. *J. Phys. Chem. Lett.* **2015**, *6* (13), 2469–2476. https://doi.org/10.1021/acs.jpclett.5b00889.

(5) Kulbak, M.; Levine, I.; Barak-Kulbak, E.; Gupta, S.; Zohar, A.; Balberg, I.; Hodes, G.; Cahen, D. Control over Self-Doping in High Band Gap Perovskite Films. *Adv. Energy Mater.* **2018**, *8* (23), 1800398. https://doi.org/10.1002/aenm.201800398.

(6) Philippe, B.; Saliba, M.; Correa-Baena, J.-P.; Cappel, U. B.; Turren-Cruz, S.-H.; Grätzel, M.; Hagfeldt, A.; Rensmo, H. Chemical Distribution of Multiple Cation (Rb^+, Cs^+, MA^+, and FA^+) Perovskite Materials by Photoelectron Spectroscopy. *Chem. Mater.* **2017**, *29* (8), 3589–3596. https://doi.org/10.1021/acs.chemmater.7b00126.

(7) McMeekin, D. P.; Sadoughi, G.; Rehman, W.; Eperon, G. E.; Saliba, M.; Hörantner, M. T.; Haghighirad, A.; Sakai, N.; Korte, L.; Rech, B.; Johnston, M. B.; Herz, L. M.; Snaith, H. J. A Mixed-Cation Lead Mixed-Halide Perovskite Absorber for Tandem Solar Cells. *Science* **2016**, *351* (6269), 151–155. https://doi.org/10.1126/science.aad5845.

(8) Ginsburg, A.; Keller, D. A.; Barad, H. N.; Rietwyk, K.; Bouhadana, Y.; Anderson, A.; Zaban, A. One-Step Synthesis of Crystalline Mn_2O_3 Thin Film by Ultrasonic Spray Pyrolysis. *Thin Solid Films* **2016**, *615*, 261–264. https://doi.org/10.1016/j.tsf.2016.06.050.

(9) Levine, I.; Gupta, S.; Brenner, T. M.; Azulay, D.; Millo, O.; Hodes, G.; Cahen, D.; Balberg, I. Mobility–Lifetime Products in $MAPbI_3$ Films. *J. Phys. Chem. Lett.* **2016**, *7* (24), 5219–5226. https://doi.org/10.1021/acs.jpclett.6b02287.

(10) San, G.; Balberg, M.; Jedrzejewski, J.; Balberg, I. The Phototransport in Halide Perovskites: From Basic Physics to Applications. *J. Appl. Phys.* **2020**, *127* (8), 085103. https://doi.org/10.1063/1.5095190.